Available online at www.sciencedirect.com

ScienceDirect

IFAC PapersOnline CONFERENCE PAPER ARCHIVE

IFAC PapersOnLine 55-31 (2022) 427–432

Limiting reactive power flow peaks in wave energy systems ⋆

Jitendra K. Jain * **Oliver Mason** * **Hafiz A. Said** *
John V. Ringwood *

* *Centre for Ocean Energy Research, Maynooth University, Ireland (e-mail: john.ringwood@mu.ie).*

Abstract: Optimal control of wave energy converters has been shown to require an injection of power into the WEC system to maintain an optimal velocity profile. While this consumption of power results in an overall increase in energy capture, it also brings more stringent requirements on the power take-off (PTO) system. Specifically, the PTO must cater for bi-directional power flow and a source available for the provision of this reactive power, either via a storage device, or the electrical grid itself. However, one aspect which has received relatively little attention is the magnitude of the reactive power peaks, which may have implications for the required overall power rating of the system. In particular, though reactive power flow may only be required for a small fraction of the wave period, reactive power peaks well in excess of active power levels bring a potentially significant capital cost in terms of system power rating, along with a unfavourable capacity factor rating. This paper examines the circumstances under which reactive power flow peaks exceed active power levels and proposes a solution which puts a finite (nonzero) limit on reactive power flow, consistent with active power levels. The problem is solved as a nonlinear constrained optimisation problem, while the consequences of imposing such a limit on energy capture are also examined.

Keywords: Wave energy, optimal control, reactive power, constrained optimisation

1. INTRODUCTION

The importance of energy-maximising control to the economic performance of wave-energy converters (WECs) has been well articulated (e.g. (Chang et al., 2018)). The control challenge is to fully utilise the operational envelope of the WEC, while respecting the physical constraints on the system. Usually, the constraints considered focus on the physical tolerances of displacement (especially regarding end-stops on linear generators), power take-off (PTO) force constraints, and there may be additional limitations on PTO/WEC velocity. In general, choice of the power rating on the PTO is a complex calculation, which considers the capital cost of the generator/PTO system, along with the likely capacity factor attained at a particular wave site evaluated by using a scatter plot of the statistical occurrence of various sea states. Ultimately, a power limit is also set by the product of force and velocity constraints (if present).

A wide variety of control philosophies have been proposed for wave energy converters (Ringwood et al., 2014), many of which (Faedo et al., 2017) can respect the hard constraints on displacement, force and (where present) velocity. These (force, velocity, displacement) present as linear constraints and, while somewhat complicating the calculation of the optimal control, can still result in a convex optimisation problem.

WEC controllers can be broadly divided into those that can inject power into the WEC system (from the grid, or some storage device), termed reactive controllers, or those that have no facility to inject power, termed passive controllers. Reactive controllers have significantly more potential to harness energy, but have extra capital costs associated to facilitate four quadrant (velocity/force) operation. Since reactive power is only employed for a small part of the wave (or pseudo wave, in panchromatic seas) cycle, it is tempting to ignore the specific requirements of reactive power flow, assuming that they are covered by forward power capacity specifications and design considerations, mentioned above. However, a number of studies (e.g. (Shek et al., 2008)) have shown that reactive power peaks can significantly exceed those for active power, with consequent implications for the power rating of the PTO system.

This paper examines the conditions under which significant reactive power peaks occur, under reactive control, and provides a solution in the form of a finite (non-zero) limit on reactive power. Specifically, there is a strong case to be made to reduce reactive power peaks to a level anticipated from forward (active) power flow, and ultimately being part of the power design specification of the WEC/PTO system, as articulated previously. However, the consequences of any reductions in reactive power limits on overall WEC energy capture need to be carefully examined, in order to fully assess the economic trade-off between power capacity specification (capital cost) and energy capture.

⋆ This work was supported by Science Foundation Ireland under Grant number 20/US/3687 and SFI Research Centre for Energy, Climate and Marine (MaREI), under grant No. 12/RC/2302_P2

10.1016/j.ifacol.2022.10.465

The remainder of the paper is laid out as follows: Section 2 describes the WEC system studied, its mathematical model, and the formulation of the optimal control problem; Section 3 recalls relevant details on the Fourier pseudospectral method; Section 4 outlines the numerical approach to solving the control problem; Section 5 examines conditions under which reactive power flow can become significant; Section 6 provides a brief discussion of the impact of imposing a constraint on reactive power on the system's performance; finally, Section 7 presents the conclusions of the study.

2. WEC SYSTEM AND MATHEMATICAL MODEL

2.1 WEC system description

For the purposes of this study, a heaving point absorber (HPA) is adopted, as shown in Fig.1. In particular, the value of reactive control is especially relevant with resonating WEC devices, explaining the choice of particular WEC type. For simplicity, we assume that the device moves in heave only, limiting the analysis, and subsequent control design, to one degree of freedom (DoF). The PTO system exerts a force $f_{PTO}(t)$, possibly using a linear generator (but not limited to such a PTO) which can be either positive or negative with respect to the sign of the WEC velocity $\dot{\gamma}(t)$.

The parameters of the HPA are taken from (Bacelli and Ringwood, 2014) corresponding to a vertical cylinder of radius $r = 4$ m and draught $d = 10$ m.

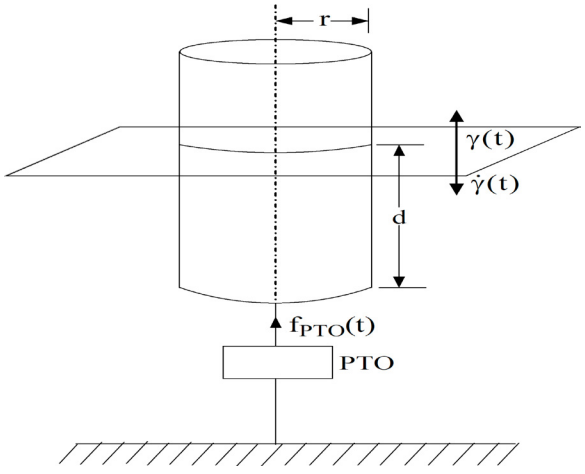

Fig. 1. Heaving point absorber.

2.2 WEC mathematical model

Using Cummins' equation (Cummins (1962)), a heaving point absorber model is given as

$$(m_b + m_\infty)\,\ddot{\gamma}(t) + b\dot{\gamma}(t) + \int_0^t k(t-\tau)\dot{\gamma}(\tau)d\tau + s\gamma(t) = f_{pto}(t) + f_e(t) \tag{1}$$

where m_b is the generalized mass, m_∞ is the added mass at infinite frequency, $\gamma(t) \in \mathbb{R}$ is the WEC displacement, b is a linear damping term corresponding to viscous drag, s is the stiffness constant, $k(t)$ is a continuous function in $[0, \alpha)$, $\alpha \leq \infty$; the convolution term $\int_0^t k(t-\tau)\dot{\gamma}(\tau)d\tau$ is a radiation force, $f_{PTO}(t)$ and $f_e(t)$ are the PTO force and excitation force, respectively. $f_e(t)$ is assumed to be continuous.

2.3 Control objective and formulation

The objective function over the time interval [0,T] for the WEC optimal control problem is given by

$$J = -\int_0^T \dot{\gamma}(t) f_{pto}(t)dt. \tag{2}$$

The optimal control problem seeks to maximise the total absorbed energy J over $[0, T]$. In this work, a reactive loading based control technique is considered. As the wave frequency varies above or below the resonance frequency of (2), the PTO force absorbs power. Such power is utilized to resonate (2) with the incident waves. The absorbed power by the PTO device (a electrical generator), can lead to large negative peaks in the output power, referred to as reactive power. For several wave conditions, the magnitude of the negative power peaks may increase above the forward power peaks. In order to handle this, the PTO ratings may need to be very high, adding additional costs. With this in mind, it is natural to consider introducing a reactive power constraint, such as the following, in the problem formulation.

$$\dot{\gamma}(t) f_{pto}(t) \leq P_R^{max} \tag{3}$$

where $P_R^{max} \in [0, \infty)$.

Practical systems modelled by (1) will have physical limitations on the values of $\gamma(t)$, and $f_{PTO}(t)$. These are defined as follows.

$$|\gamma(t)| \leq g_{max}, \quad |f_{PTO}(t)| \leq f_{max} \tag{4}$$

Now, the optimal control problem is to maximise J in (2) by designing an appropriate $f_{pto}(t)$ subject to (1), (3), and (4).

To write the problem in state-space form, define $x_1(t) = \gamma(t)$, $x_2(t) = \dot{\gamma}(t)$, and $u(t) = f_{pto}(t)$. Then, the model becomes

$$\begin{aligned} \dot{x}_1 &= x_2 \\ m\dot{x}_2 &= -bx_2 - \int_0^t k(t-\tau)x_2(\tau)d\tau - sx_1 + u + f_e \end{aligned} \tag{5}$$

where $m = m_b + m_\infty$.

From (2), the objective function is

$$J = -\int_0^T x_2 u dt, \tag{6}$$

and the constraints are rewritten as

$$x_2 u \leq P_R^{max}, \qquad |x_1| \leq g_{max}, \qquad |u| \leq f_{max} \tag{7}$$

3. FOURIER PSEUDOSPECTRAL METHOD

The constrained optimal control problem described in the previous section can be solved numerically using a Fourier pseudospectral method following the framework presented in Bacelli and Ringwood (2015). The functions describing the state variables x_1, x_2 and control input u are approximated by zero mean truncated Fourier series;

the excitation force f_e is also assumed to be zero-mean. The dynamics, objective function, and constraints are then expressed in terms of the coefficients of the Fourier expansions, leading to a finite dimensional optimisation problem. In this section, the construction of a finite dimensional approximation of the state variables solving the dynamical equations (5) is outlined. The objective function, constraints, and solution of the optimal control problem are addressed in the next section.

In terms of the standard Fourier basis functions, the state and control approximations are given by:

$$\begin{aligned} x_j(t) &\approx \sum_{r=1}^{N/2} x_{jr}^c cos(r\omega_o t) + x_{jr}^s sin(r\omega_o t) = \Psi(t)\hat{x}_j \\ u(t) &\approx \sum_{r=1}^{N/2} u_r^c cos(r\omega_o t) + u_r^s sin(r\omega_o t) = \Psi(t)\hat{u} \end{aligned} \tag{8}$$

where $j = 1, 2$, $\omega_o = \frac{2\pi}{T}$ is the fundamental frequency, and

$$\begin{aligned} \hat{x}_j &= \left[x_{j1}^c, x_{j1}^s, \ldots, x_{j\frac{N}{2}}^c, x_{j\frac{N}{2}}^s\right]^T \\ \hat{u} &= \left[u_1^c, u_1^s, \ldots, u_{\frac{N}{2}}^c, u_{\frac{N}{2}}^s\right]^T \\ \Psi(t) &= \left[cos(\omega_o t), sin(\omega_o t), \ldots, cos\left(\frac{N}{2}\omega_o t\right), sin\left(\frac{N}{2}\omega_o t\right)\right] \end{aligned}$$

The orthogonality of the Fourier basis functions with respect to the standard inner product in $L^2([0,T])$ can be used to show that

$$\int_0^T \Psi^T(t)\Psi(t)dt = \frac{T}{2} I_N \tag{9}$$

where I_N is the identity matrix of size N.

Using this, the energy is approximated by

$$J^N = -\int_0^T \hat{u}^T \Psi^T(t)\Psi(t)\hat{x}_2 dt = -\frac{T}{2}\hat{u}^T\hat{x}_2 \tag{10}$$

The derivatives of x_j, $j = 1, 2$ can be written as

$$\dot{x}_j^N = \dot{\Psi}(t)\hat{x}_j = \Psi(t) D_\Psi \hat{x}_j \tag{11}$$

where $D_\Psi \in \mathbb{R}^{N\times N}$ is a block diagonal matrix, given by

$$D_\Psi = \begin{bmatrix} 0 & \omega_o & 0 & \cdots & 0 & 0 \\ -\omega_o & 0 & 0 & \cdots & 0 & 0 \\ 0 & 0 & \ddots & & \vdots & \vdots \\ \vdots & \vdots & & \ddots & 0 & 0 \\ 0 & 0 & \cdots & 0 & 0 & \frac{N\omega_o}{2} \\ 0 & 0 & \cdots & 0 & -\frac{N\omega_o}{2} & 0 \end{bmatrix} \tag{12}$$

Using (11), the following approximation of the dynamics (5) is obtained.

$$\begin{aligned} \Psi(t)D_\Psi\hat{x}_1 =& \Psi(t)\hat{x}_2 \\ m\Psi(t)D_\Psi\hat{x}_2 =& -b\Psi(t)\hat{x}_2 - s\Psi(t)\hat{x}_1 \\ & - \int_{-\infty}^t k(t-\alpha)\Psi(t)\hat{x}_2 d\alpha \\ & + \Psi(t)\hat{u} + f_e \end{aligned} \tag{13}$$

Equating coefficients in the first state equation in (13) yields

$$D_\Psi \hat{x}_1 = \hat{x}_2 \tag{14}$$

Since D_Ψ is invertible,

$$\hat{x}_1 = D_\Psi^{-1}\hat{x}_2 \tag{15}$$

where

$$D_\Psi^{-1} = \begin{bmatrix} 0 & -\frac{1}{\omega_o} & 0 & \cdots & 0 & 0 \\ \frac{1}{\omega_o} & 0 & 0 & \cdots & 0 & 0 \\ 0 & 0 & \ddots & & \vdots & \vdots \\ \vdots & \vdots & & \ddots & 0 & 0 \\ 0 & 0 & \cdots & 0 & 0 & -\frac{2}{N\omega_o} \\ 0 & 0 & \cdots & 0 & \frac{2}{N\omega_o} & 0 \end{bmatrix}$$

The residual form of the second equation in (13) is given by

$$\begin{aligned} w_2^N =& m\Psi D_\Psi \hat{x}_2 + b\Psi\hat{x}_2 + s\Psi\hat{x}_1 \\ & + \int_{-\infty}^t k(t-\alpha)\Psi(t)\hat{x}_2 d\alpha - \Psi\hat{u} - f_e, \end{aligned} \tag{16}$$

and the residual error is thus minimised by solving

$$\left\langle \Psi^T, w_2^N \right\rangle = \mathbf{0} \tag{17}$$

where $\mathbf{0} \in \mathbb{R}^N$.

Taking the inner product of Ψ^T with each term in (16) separately yields

$$\begin{aligned} \left\langle \Psi^T, m\Psi D_\Psi \hat{x}_2 \right\rangle =& m\vartheta D_\Psi \hat{x}_2 = \frac{T}{2} m I_N D_\Psi \hat{x}_2, \\ \left\langle \Psi^T, b\Psi\hat{x}_2 \right\rangle =& \frac{T}{2} b I_N \hat{x}_2, \\ \left\langle \Psi^T, s\Psi\hat{x}_1 \right\rangle =& \frac{T}{2} s I_N \hat{x}_1, \\ \left\langle \Psi^T, \Psi\hat{u} \right\rangle =& \frac{T}{2} I_N \hat{u}, \\ \left\langle \Psi^T, f_e \right\rangle =& \frac{T}{2} I_N \hat{e}, \end{aligned} \tag{18}$$

where $\hat{e}$ is the vector of Fourier coefficients of f_e.

Substituting (15) into (18) shows that

$$\left\langle \Psi^T, s\Psi\hat{x}_1 \right\rangle = \frac{T}{2} s I_N D_\Psi^{-1}\hat{x}_2 \tag{19}$$

Representing the convolution integral in terms of the coefficient vectors requires additional manipulation and we do not include the details here due to space constraints. A full description of how to include this term can be found in Bacelli and Ringwood (2015). The key point is that combining (17) with the expressions obtained for the separate inner products in the residual leads to the following equation for $\hat{x}_2$.

$$H\hat{x}_2 = \hat{u} + \hat{e} \tag{20}$$

Here H is a block-diagonal matrix, of the form

$$H = \begin{bmatrix} b_1 & m_1 & 0 & \cdots & 0 & 0 \\ -m_1 & b_1 & 0 & \cdots & 0 & 0 \\ 0 & 0 & \ddots & & \vdots & \vdots \\ \vdots & \vdots & & \ddots & 0 & 0 \\ 0 & 0 & \cdots & 0 & b_{N/2} & m_{N/2} \\ 0 & 0 & \cdots & 0 & -m_{N/2} & b_{N/2} \end{bmatrix} \tag{21}$$

where the diagonal elements in H, b_r, $1 \le r \le N/2$ are all positive.

As the matrix H is clearly invertible as the determinant of each block on the diagonal is $b_r^2 + m_r^2 > 0$, we have that

$$\hat{x}_2 = H^{-1}\hat{u} + H^{-1}\hat{e}. \tag{22}$$

Combining this with (15) gives the approximate solution for the states x_1, x_2. In the next section, the solution of the optimal control problem, based on these, is described.

4. CONTROL SOLUTION

To solve the optimal control problem using the Fourier pseudospectral method, it is necessary to express the objective function J and the other constraints in terms of the coefficient vectors $\hat{u}$, $\hat{x}_1$, $\hat{x}_2$.

First, using equation (6) the objective function for the finite dimensional approximation is given by

$$J = -\int_0^T \hat{u}^T \Psi^T \Psi \hat{x}_2 dt = -\frac{T}{2}\hat{u}^T \hat{x}_2 \tag{23}$$

Using (22), this can be written as

$$J = -\frac{T}{2}\hat{u}^T H^{-1}\hat{u} - \frac{T}{2}\hat{u}^T H^{-1}\hat{e} \tag{24}$$

Unconstrained Case

As all the diagonal elements in (21) are positive. It follows that the matrix $H + H^T$ is positive definite so the total absorbed energy in (24) is concave, and the optimal control u^*, which maximises (24) in the absence of constraints is

$$\hat{u}^* = \left(H^{-1} + H^{-T}\right)^{-1} H^{-1}\hat{e} \tag{25}$$

Handling Constraints

To obtain a finite dimensional approximation of the constrained optimal control problem, it is necessary to express the constraints in (7) in terms of the Fourier coefficients.

The constraint on the control input becomes

$$|\Psi(t)\hat{u}| \leq f_{max}. \tag{26}$$

Using the expressions (22) and (15), we can write the constraint on $x_1(t)$ as

$$|\Psi(t)D_\Psi^{-1}H^{-1}(\hat{u} + \hat{e})| \leq g_{max}. \tag{27}$$

The constraint $x_2 u \leq P_R^{max}$ is approximated by

$$\hat{u}^T \Psi(t)^T \Psi(t)\hat{x}_2 \leq P_R^{max} \tag{28}$$

After substituting (22) into (28), we have

$$\hat{u}^T \Psi(t)^T \Psi(t) H^{-1}\hat{u} + \hat{u}^T \Psi(t)^T \Psi(t) H^{-1}\hat{e} \leq P_R^{max}. \tag{29}$$

The constraints in (26), (27), (29) are all point-wise constraints on truncated Fourier series. Due to the difficulty of determining extrema for such series, the constraints are enforced at a finite set of points $\{t_k\}_{k=0}^{N_c}$ in $[0, T]$. Writing Ψ_k for $\Psi(t_k)$, we end up with $N_c + 1$ constraints

$$\hat{u}^T \Psi_k^T \Psi_k H^{-1}\hat{u} + \hat{u}^T \Psi_k^T \Psi_k H^{-1}\hat{e} - P_R^{max} \leq 0. \tag{30}$$

The above discussion shows how to transcribe the original optimal control problem to a finite dimensional, constrained, nonlinear optimisation problem defined by the objective function (24) and the constraints (26), (27), (30). In the results described in the following sections, the finite dimensional problem was solved using the primal-dual interior point algorithm implementation in the CasADi toolbox for Matlab (Andersson et al., 2019).

5. REACTIVE POWER FLOW ANALYSIS

In this section, we examine the conditions under which reactive power flow becomes significant, with particular focus on the predominant wave period relative to the device resonant period; in general, significant amounts of reactive power are required when the device resonant period is greater (i.e. the device is slower) than the predominant wave period. In contrast, slowing a device with fast dynamics to a longer wave period can be achieved with increased PTO loading.

We also examine the impact of physical system constraints on the use of reactive power and the (linearised) viscous drag term is also varied to analyse the effect of dynamic drag on reactive power flow.

We employ a Jonswap spectrum (Hasselmann et al., 1973), with an example spectrum shown in Fig.2. The employment of a JONSWAP spectrum gives the option to experiment with the spectral bandwidth of the sea spectrum, via the JONSWAP peak enhancement factor, γ_J.

For a HPA WEC, such as that shown in Fig.1, the most significant constraints on the system are force and displacement, both directly related to the PTO physical constraints. Figs.3-5. Clearly, the impact on the ratio of reactive to forward power (P_r/P_f) is minimal, while the force constraint has a significant impact, up to a certain point (around 2 x 10^6 N, though somewhat dependent on the peak wave period, T_p). The dominance of the force constraint is probably to be expected, since force forms one of the component factors of power (the other being velocity).

Fig.6 shows the P_r/P_f ratio for the unconstrained case, for various values of T_p and the (linearised) viscous drag coefficient b. We can note that, for some combinations of T_p and b, the P_r/P_f ratio can significantly exceed unity, indicating that the peaks in reactive power flow are greater than those for active (forward) power flow.

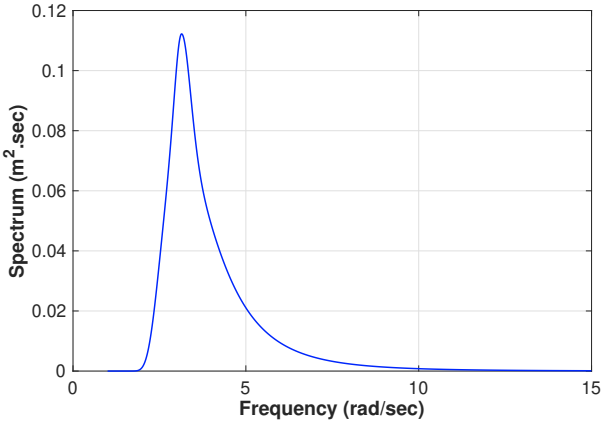

Fig. 2. Jonswap wave spectrum employed, with $T_p = 2sec$, peak enhancement factor, γ_J=1.5, and significant wave height H_s=2 m.

6. IMPACT OF REACTIVE POWER LIMIT

Initially, we examine a particular evolution of the system power flow, for conditions corresponding to no reactive

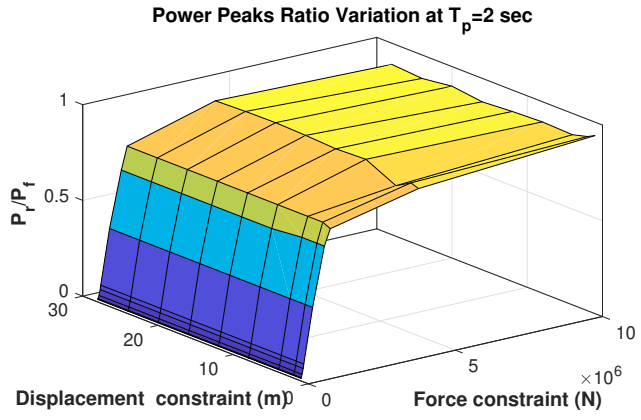

Fig. 3. Power peak ratio variation with displacement and PTO force constraints at $T_p = 2sec$.

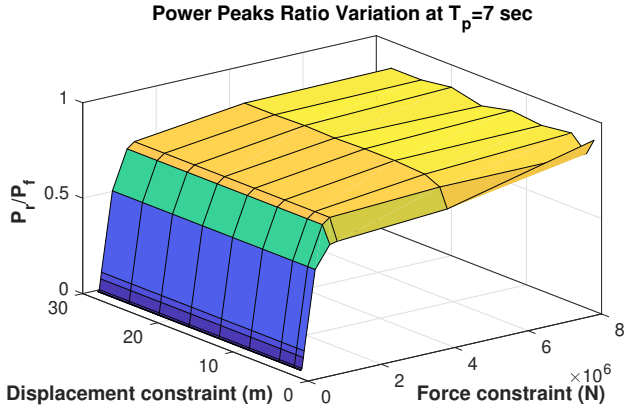

Fig. 4. Power peak ratio variation with displacement and PTO force constraints at $T_p = 7sec$.

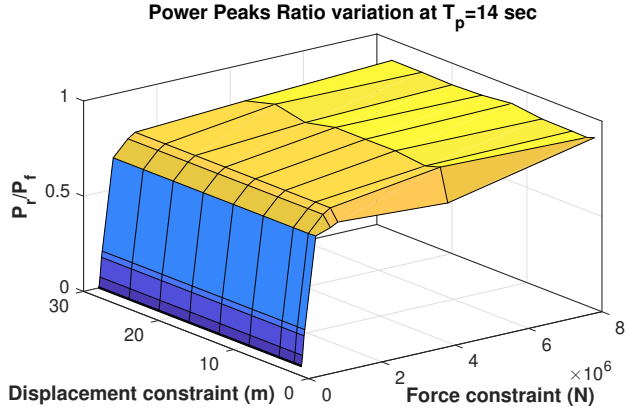

Fig. 5. Power peak ratio variation with displacement and PTO force constraints at $T_p = 14sec$.

power flow constraint, and then applying a constraint on P_r of 1 x 10^6 W, shown in Fig.7. The other parameters for this simulation are $T_p = 9$ sec, significant wave height $H_s = 2m$, peak enhancement factor, γ_J=1.5, damping, b=10 N.sec/m, displacement constraint =2.5 m and velocity constraint =2.5 m/sec. Total energy obtained (over the simulation duration) without applying the reactive power constraint is 1.7896e+07 J, with 1.3397e+07 J converted

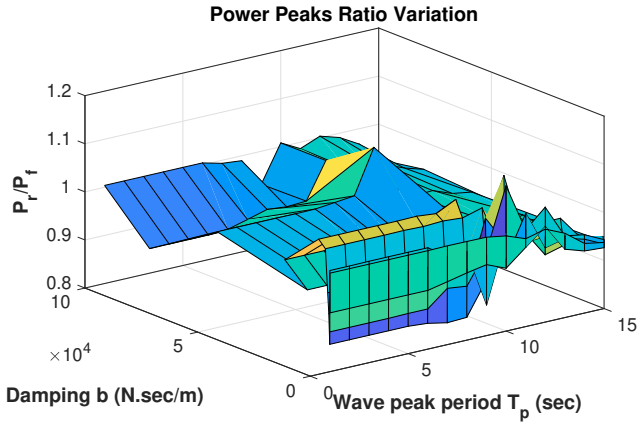

Fig. 6. Power peak ratio variation with damping b and peak period T_p.

following application of the constraint. Note that the limit on P_r (of 1 x 10^6) is strictly observed.

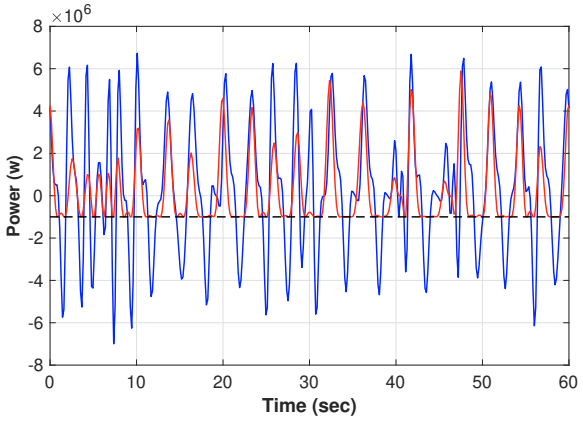

Fig. 7. Power variation with time: without reactive power constraint (solid line, blue color) and with reactive power constraint (solid line, red colour).

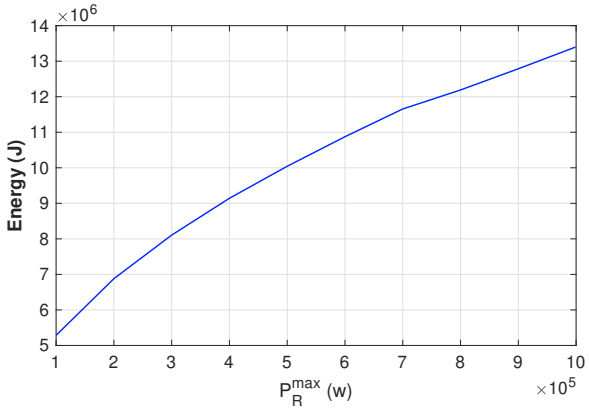

Fig. 8. Energy capture increase with progressive relaxation of reactive power constraint.

Fig.8 demonstrates the incremental impact of a reactive power constraint on overall energy capture. While the energy capture for larger values of P_R^{max} were difficult to achieve, due to convergence issues, the generally asymptotic behaviour of Fig.8 suggests that there is a diminishing return on providing increasing values of PTO power ca-

pacity to facilitate reactive power peaks, especially where these peaks may be in excess of the active/forward power peaks.

7. CONCLUSION

This preliminary study, to the best of the authors' knowledge, is unique in examining the conditions under which reactive power peaks occur, and provides a technical mechanism to provide an optimal PTO control with a strict limit on reactive power levels (i.e. optimal constrained control). An alternative practical solution would be to calculate the optimal control and then try to limit reactive power flow, via saturation characteristics applied to the velocity and force signals. However, since velocity is a system variable, imposing any velocity limit would require some advance consideration of the system dynamics.

A further possibility is to use an optimal constrained control solution which considers the combination of velocity and force constraints to limit excessive peaks in reactive power. One advantage of this is that both force and velocity constraints are linear, while any power constraint is nonlinear, with consequent convergence problems for the control calculation. However, while aligning the product of force and velocity constraints with the power constraints guarantees the power constraint, it may hinder the individual freedom of either velocity or force in providing a truly optimal control while remaining within the power constraint. Nevertheless, the use of individual force and velocity constraints to provide an overall power constraint will be investigated as an area for future work, since the relative ease with which the linearly constrained optimal control solution is achieved may trump any theoretically optimal (nonlinearly) power constrained solution which may be not always be achievable.

The preliminary results reported in this paper do, however, demonstrate the possibility to limit reactive power in an optimal way, especially so that the reactive power peaks do not determine the required power capacity of the PTO system. Given the (projected) asymptotic nature of Fig.8, a reduction in the allowable reactive power level to the typical (rated) active/forward system power seems sensible, and the marginal loss in captured energy is likely to be more than compensated for in the reduced capital cost of the PTO system. The paper also examines the conditions under which reactive power peaks can exceed active/forward power peaks, dependent on the relative positioning of peak wave period and device resonant period, as well as the level of viscous damping. The effect of the viscous damping parameter is interesting, since the value of b may be indicative of the WEC device type, as well as more subtle variations, due to the particular WEC model, with a type classification. For example, for large b values, Fig.6 shows that the P_r/P_f ratio tends towards unity, with no excess of reactive power peak over the active/forward limits, obviating the need for a specific reactive power flow limit. This suggests that resonating WECs (e.g. HPAs) may have more need for a specific reactive power flow limit than, say, oscillating wave surge converters (OWSCs), which have typically higher viscous drag coefficients.

Finally, it is envisaged that the control solution presented here would be implemented in a receding-horizon fashion, such as in (Genest and Ringwood, 2016). For a full-scale WEC, the sampling interval would be of the order of $\sim$ 0.1-1 s, which is likely achievable with an embedded implementation of the proposed algorithm. Over the control horizon, an estimate and forecast of the wave excitation force is needed (perfect knowledge of this is assumed in the current analysis, for simplicity), which could be provided by a range of methods, such as those reported in (Peña-Sanchez et al., 2019) and (Pena-Sanchez et al., 2018).

REFERENCES

Andersson, J.A.E., Gillis, J., Horn, G., Rawlings, J.B., and Diehl, M. (2019). CasADi – A software framework for nonlinear optimization and optimal control. *Mathematical Programming Computation*, 11(1), 1–36. doi: 10.1007/s12532-018-0139-4.

Bacelli, G. and Ringwood, J.V. (2015). Numerical optimal control of wave energy converters. *IEEE Trans. Sustain. Energy*, 6(2), 294–302.

Bacelli, G. and Ringwood, J.V. (2014). Numerical optimal control of wave energy converters. *IEEE Transactions on Sustainable Energy*, 6(2), 294–302.

Chang, G., Jones, C.A., Roberts, J.D., and Neary, V.S. (2018). A comprehensive evaluation of factors affecting the levelized cost of wave energy conversion projects. *Renewable energy*, 127, 344–354.

Cummins, W. (1962). The impulse response function and ship motions. *Schiffstechnik*, 9, 101–109.

Faedo, N., Olaya, S., and Ringwood, J.V. (2017). Optimal control, MPC and MPC-like algorithms for wave energy systems: An overview. *IFAC Journal of Systems and Control*, 1, 37–56.

Genest, R. and Ringwood, J.V. (2016). Receding horizon pseudospectral control for energy maximization with application to wave energy devices. *IEEE Transactions on Control Systems Technology*, 25(1), 29–38.

Hasselmann, K., Barnett, T.P., Bouws, E., Carlson, H., Cartwright, D.E., Enke, K., Ewing, J., Gienapp, A., Hasselmann, D., Kruseman, P., et al. (1973). Measurements of wind-wave growth and swell decay during the joint north sea wave project (JONSWAP). *Ergaenzungsheft zur Deutschen Hydrographischen Zeitschrift, Reihe A*, A8(12).

Pena-Sanchez, Y., Mérigaud, A., and Ringwood, J.V. (2018). Short-term forecasting of sea surface elevation for wave energy applications: The autoregressive model revisited. *IEEE Journal of Oceanic Engineering*, 45(2), 462–471.

Peña-Sanchez, Y., Windt, C., Davidson, J., and Ringwood, J.V. (2019). A critical comparison of excitation force estimators for wave-energy devices. *IEEE Transactions on Control Systems Technology*, 28(6), 2263–2275.

Ringwood, J.V., Bacelli, G., and Fusco, F. (2014). Energy-maximizing control of wave-energy converters: The development of control system technology to optimize their operation. *IEEE Control Syst. Mag*, 34(5), 30–55.

Shek, J., Macpherson, D., and Mueller, M. (2008). Phase and amplitude control of a linear generator for wave energy conversion. In *4th IET International Conference on Power Electronics, Machines and Drives (PEMD 2008)*, 66. IET.